Electronic Supplementary Material (ESI) for Journal of Materials Chemistry A.


# Supporting Information

**Conductive 2D dithiolene MOFs-based electrodes for low-temperature high-performance energy storage**

*Bing Wang[#a,c], Wen-Wei Song[#a], Lin Liu[a], Xue-Jun Gu[a], Zheng-Bo Han[*a], Fu-Shun Liang[*a] and Shi-Ming Wang[*b]*

*[a] College of Chemistry, Liaoning University, Shenyang 110036, P. R. China E-mail: ceshzb@lnu.edu.cn; fsliang@lnu.edu.cn*

*[b] Light Industry College, Liaoning University, Shenyang 110036, P. R. China E-mail：wangsm@lnu.edu.cn*

*[c] School of Chemistry, South China Normal University, Guangzhou, 510006, P.R. China*

*# Bing Wang and Wen-Wei Song contribute the same to this paper.*

## Summary

S1. Supporting experimental section (Supporting Figure S1~S4)

S2. Results and Discussion (Supporting Figure S5~S11).

S3. Supporting Table S1.

**Experimental Section**

**Resistivity measurement.**

Conductivity measurement was conducted using a Jingge ST2258A Semiconductor Characterization System, equipped with 2-terminal probe station at different temperature. The samples pellets prepared by isostatic pressing, the diameter of the pellets is 3.20 mm, and the thicknesses from left to right are 1.0, 1.5 and 2.0 mm.

**Electrochemical measurements and evaluations.**

The specific capacitance calculated from Cyclic voltammetry (CV) examined in the range of -0.2 to 0.8 V at 10-100mV $s^{-1}$, areal capacitance (F $cm^{-2}$) calculated by equations (1)

$$C_{cv} = \frac{\int IdV}{vs\Delta V} \qquad (1)$$

where *Ccv* is the specific capacitance, *I* (A) is the instant current, *v* (V $s^{-1}$) is the scan rate, Δ*V* (V) is the range of a scanning region, *S* ($cm^2$) is the effective electrode area.

The gravimetric capacitance of single electrodes, based on galvanostatic charge/discharge curves (*Cgal*), were also calculated using the equation (2)

$$C_{gal} = \frac{2I\Delta t}{m\Delta V} \qquad (2)$$

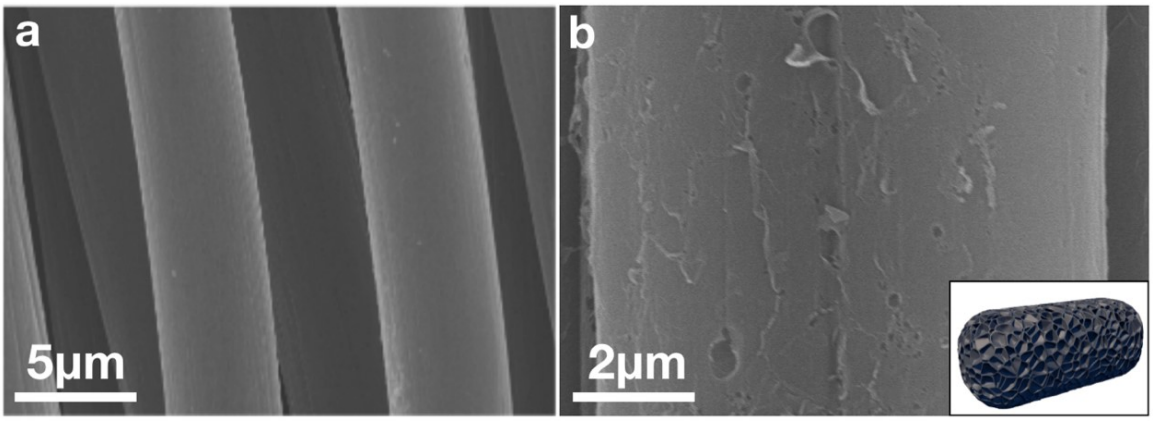


**Fig. S1** SEM image of carbon cloth substrate before (a) and after (b) high temperature puffing.

**Preparation of organic ligand.**

**2,3,6,7,10,11-Hexabromotriphenylene (HBT).** To a solution of triphenylene (1, 1.07 g, 4.7 mmol) in nitrobenzene (40 mL) with iron powder (100 mg, 1.79 mmol) bromine (2.2 mL, 38.8 mmol) was slowly added over 15 minutes. The solution was then allowed to stand for 16 hours at room temperature. It was heated at 205°C for 2 hours. The mixture was cooled to room temperature and mixed with diethyl ether (150 mL) and filtered. The crude white solid was washed by diethyl ether (3×30 mL) and acetone (3×10 mL). After drying in vacuo for 12 hours, 3.13 g of 2,3,6,7,10,11-hexabromotriphenylene (yield 95%) was collected. The product was used directly without characterization due to low solubility.

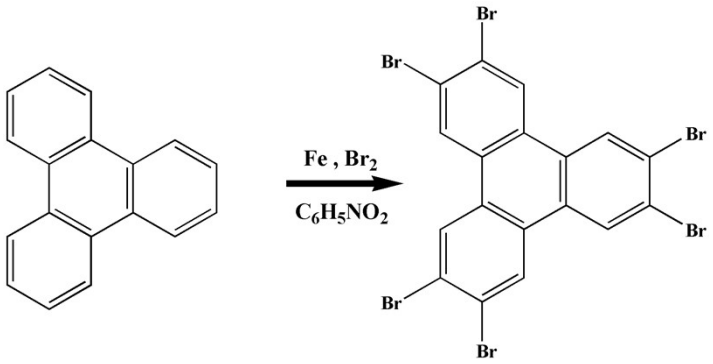


**Fig. S2** Synthetic procedure of 2,3,6,7,10,11-hexabromotriphenylene.

**2,3,6,7,10,11-Hexakis(butyrylthio)triphenylene (HBuTT).** In an $N_2$-filled glove-box, S4a magnetic stirrer, HBT (0.216 g, 0.3 mmol) and $CH_3SNa$ (0.664 g, 9.0 mmol) were loaded into a 25-ml two-neck round-bottom flask. Then the flask was connected to a Schlenk line. DMEU (anhydrous, bubbled with $N_2$, 10 ml) was transferred into the flask via cannula. The reaction mixture was then stirred at 240ºC for 48 h. After the mixture was cooled to 0ºC (first naturally to Rt., then by an ice bath), n-butyric chloride (1.24 ml, 12.6 mmol) was injected under $N_2$. After being stirred at 0ºC for 2h, the mixture was poured into ice water (50 ml) and extracted by toluene (3 x 30 ml). The combined organic layer was then washed by water (4 x 30 ml), dried over $MgSO_4$, evaporated in vacuo. The crude product (black solid) was purified by chromatography (3:1 $CH_2Cl_2$/hexane) to afford an off-white solid (168 mg, yield 67%). 1H NMR (400 MHz, $CDCl_3$): 8.50 (s, 6H), 2.71 (t, 12H), 1.82 (sextet, 12H), 1.06 (t, 18H). 13C NMR (100 MHz, $CDCl_3$): 196.56; 132.55; 132.31; 129.82; 45.55; 19.10; 13.65. Chemical analysis of the product $C_{42}H_{48}O_6S_6$ yielded the following: Calcd [C (59.97%), H (5.75%)]; Found [C (59.45%), H (5.63%)].

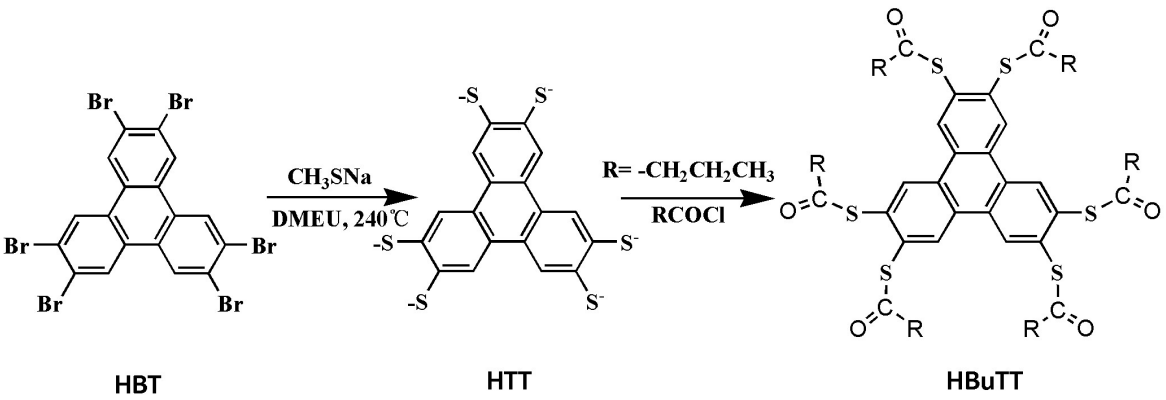


**Fig. S3** Synthesis of HBuTT.

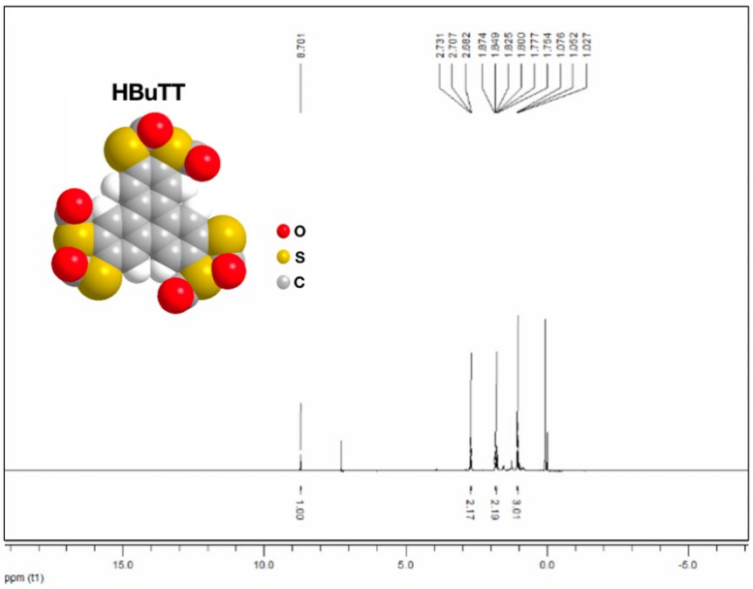


**Fig. S4** 1H-NMR spectrum of HBuTT

**Results and discussion supporting Figure S5~S11**

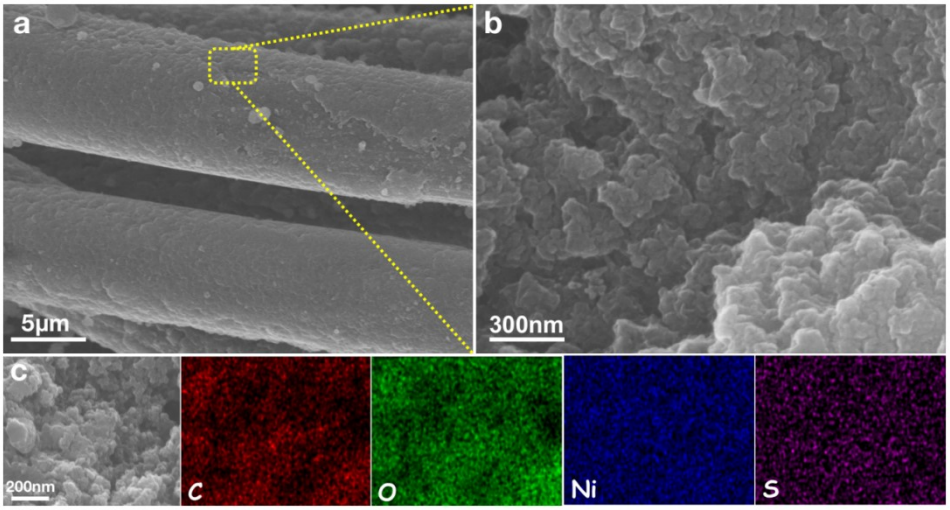


**Fig. S5** SEM image of HTTP-Ni-CC (a) and nano-particles of HTTP-Ni-CC (b); (c) EDS

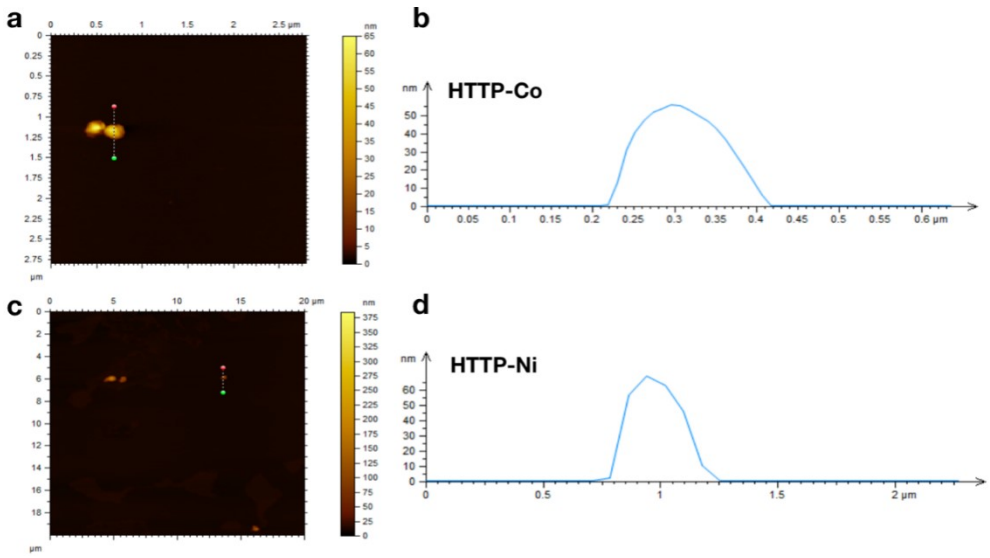


mapping for HTTP-Co-CC.

**Fig. S6** AFM images of uniform nanoparticles, 2DSP single-layer sheet after vertical transfer onto a mica wafer. (a) HTTP-Co and (c) HTTP-Ni are the height image. (b) and (d) Cross-section analysis along the dotted lines in image, respectively. The surface

roughness Ra = 0.179 nm. The crystal particle size of samples is about 50-60 nm on mica.

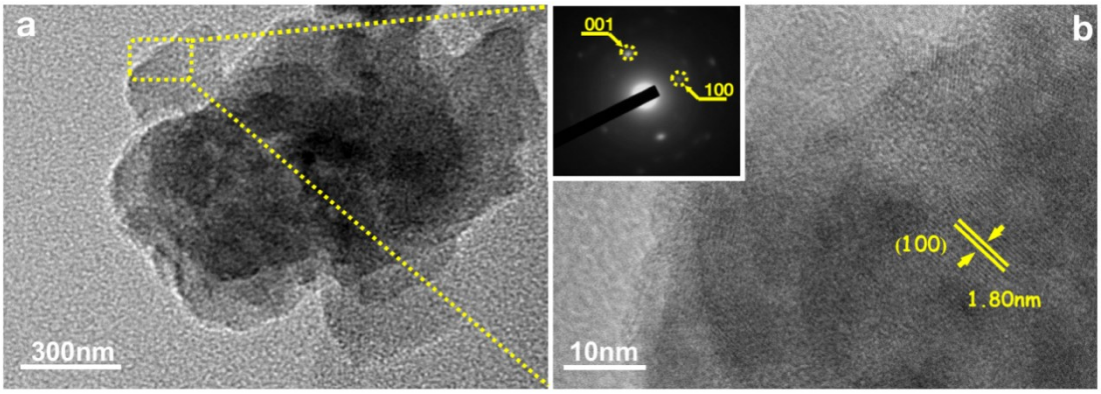


**Fig. S7** (a) TEM images of HTTP-Ni-CC; (b) Magnified section of the TEM image with the corresponding crystal lattice fringes, Inset: corresponding SAED pattern (scale bar, 10 $nm^{-1}$).

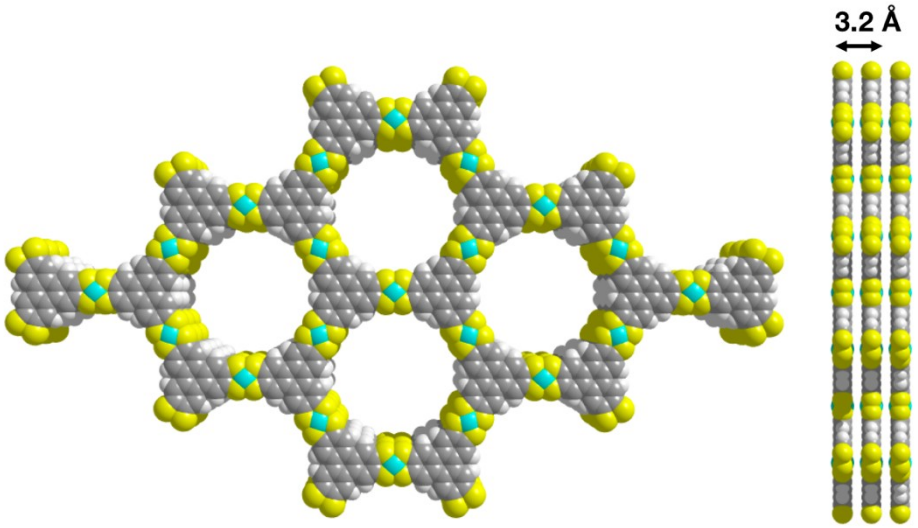


**Fig. S8** An eclipsed space-filling model of the HTTP-Ni model. yellow, grey, blue and white spheres represent S, C, Ni and H atoms, respectively; a.u.: arbitrary units.

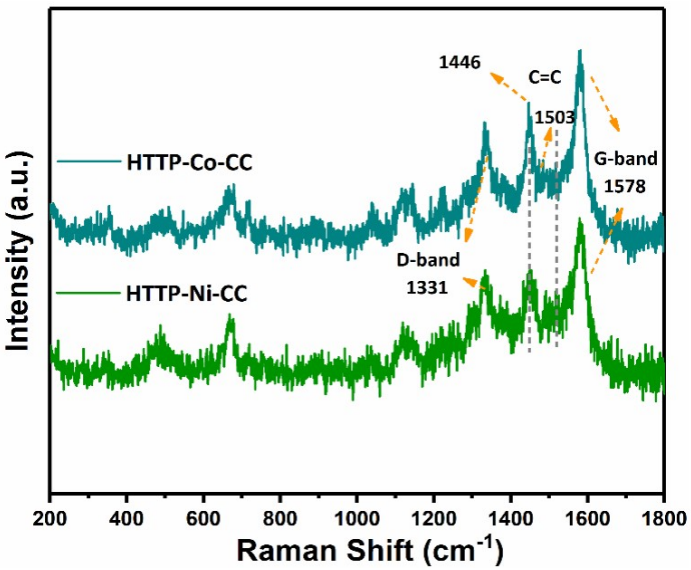


**Fig. S9** Ranman shifts of HTTP-Co-CC and HTTP-Ni-CC (cyan, green).

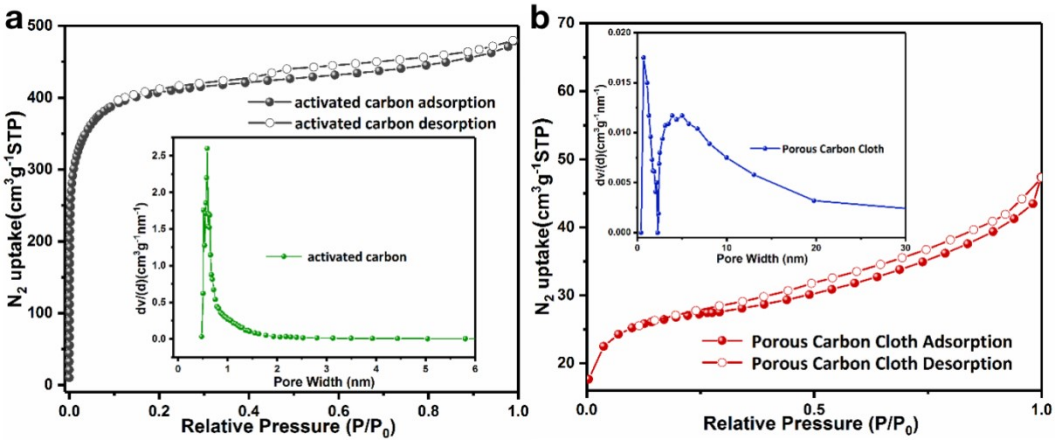


**Fig. S10** (a) $N_2$ adsorption-desorption isotherms for activated carbon, inset: Pore size distribution for activated carbon; (b) $N_2$ adsorption-desorption isotherms for porous carbon cloth, inset: Pore size distribution for porous carbon cloth.

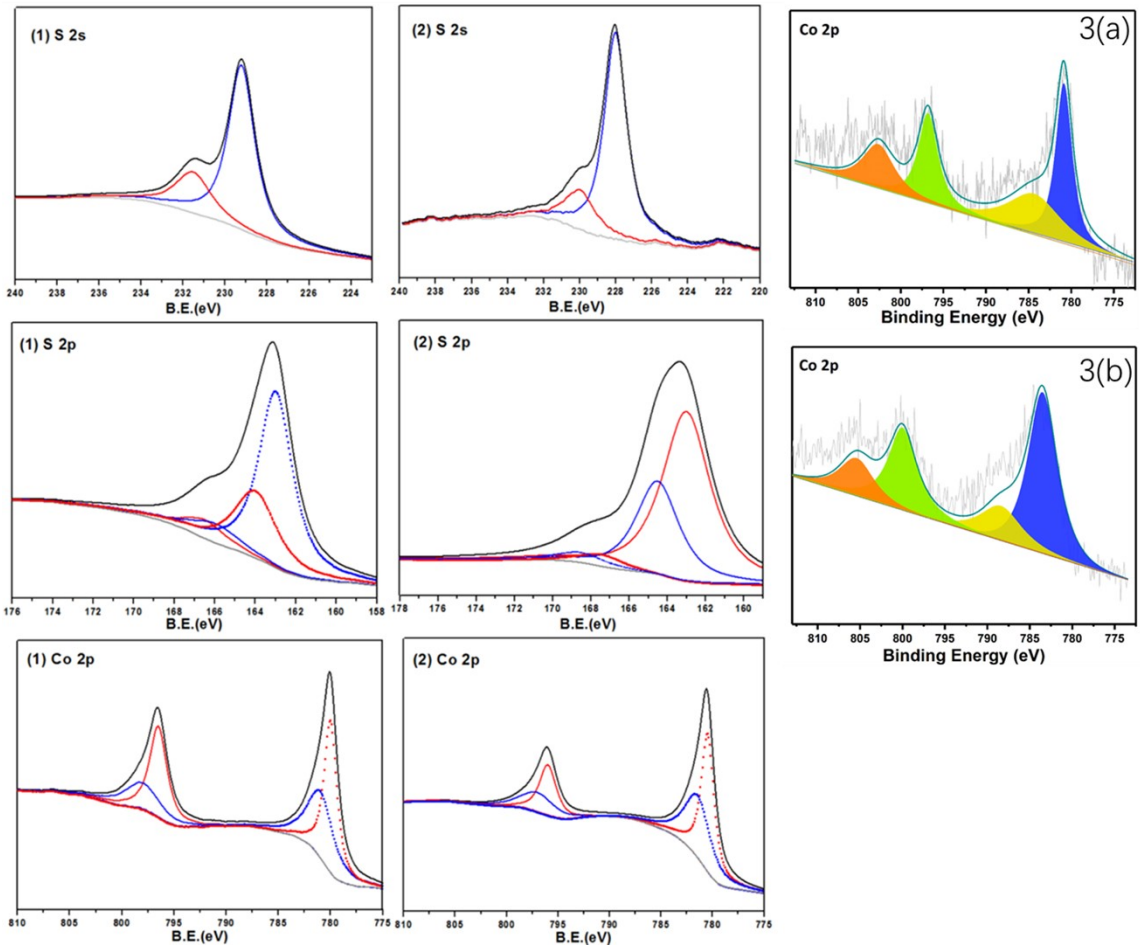


**Fig. S11** X-ray photoelectron spectroscopy (XPS) data of the cobalt dithiolene collected at room temperature (1) before and (2) after conductivity measurements. XPS data from top: (a) Co 2p, (b) S 2s, and (c) S 2p; The high-resolution XPS spectra of Co 2p before (3a) and after (3b) HTTP-Co-CC undergoing the CV measurements.

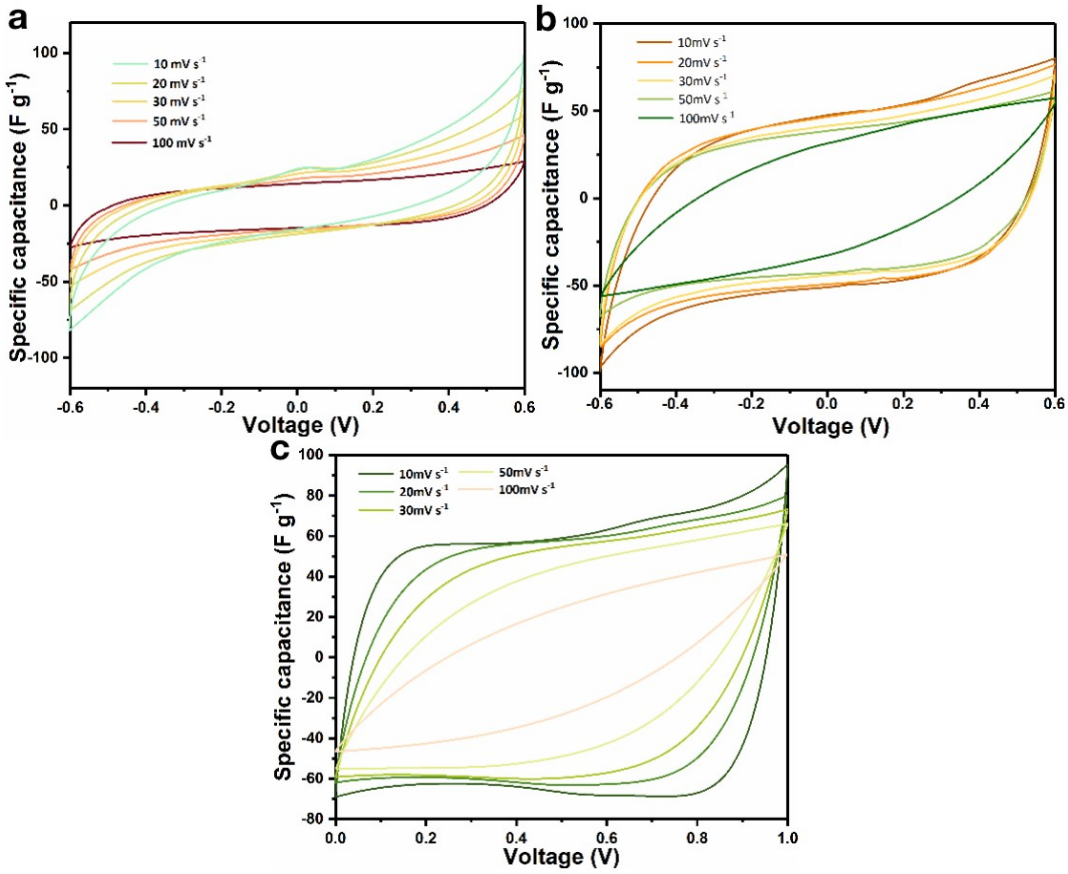


**Fig. S12** CV curves of EDLCs based on (a) HTTP-Co-CC and (b) HTTP-Ni-CC and (c) AC

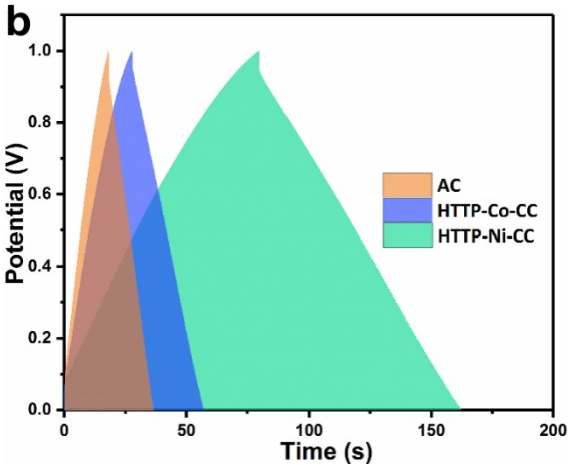


measured with different scan rate (10-100 mV $s^{-1}$) at 20°C.

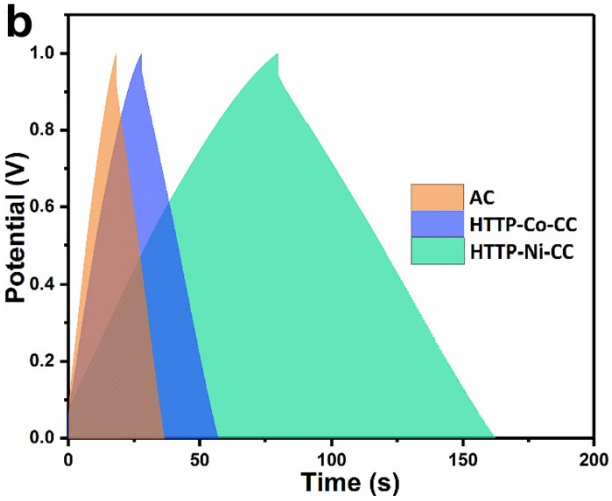


**Fig. S13** Galvanostatic charge/discharge curves of the AC, HTTP-Co-CC and HTTP-Ni-CC electrode with the current densities of 0.5 A $g^{-1}$ at -60°C.

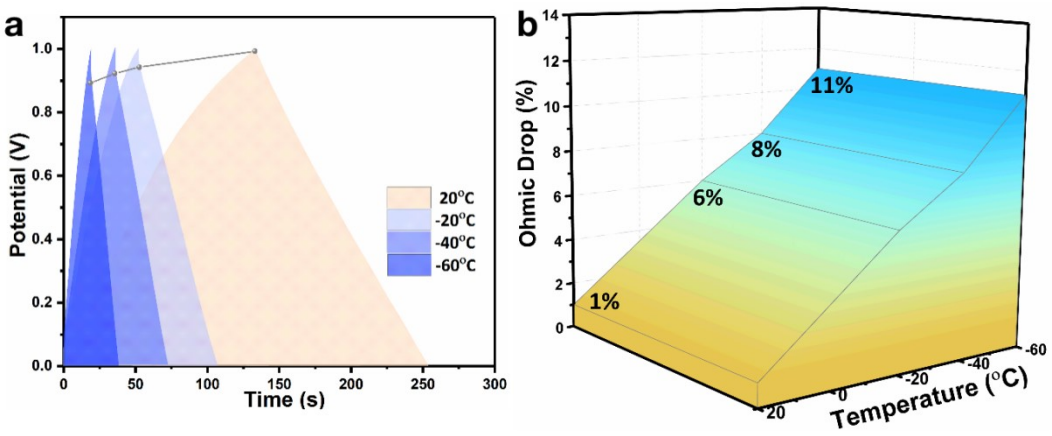


**Fig. S14** (a) Galvanostatic charge/discharge curves of the AC with the current densities of 0.5 A $g^{-1}$ at different temperature; (b) Relationship between Ohmic drop and temperature.

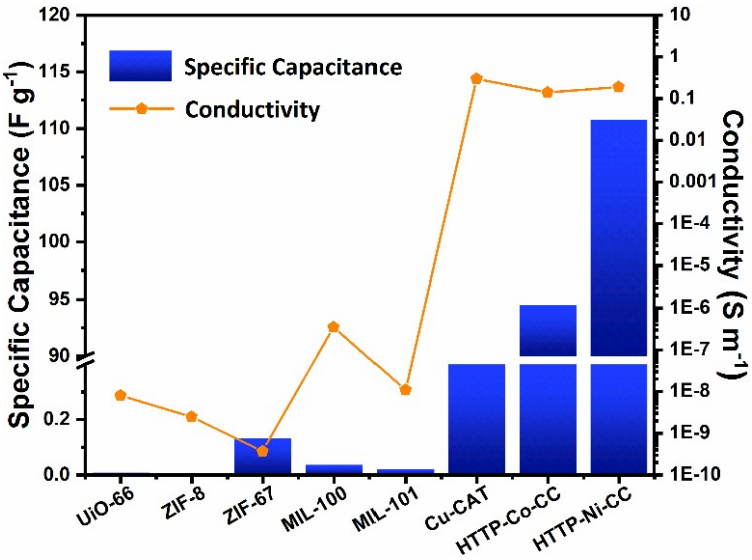


**Fig. S15** The relationship between conductivity and specific capacitance of the electrodes of different MOF materials (20°C).

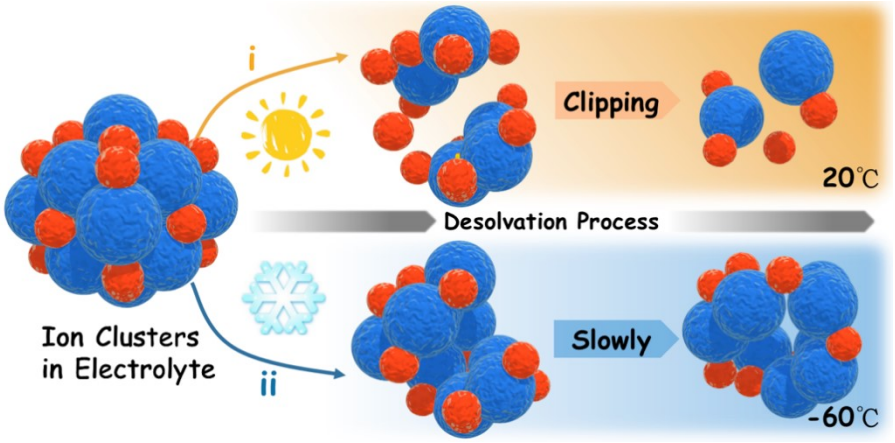


**Fig. S16** Desolvation process of electrolyte at 20°C and -60°C.

Normally, the ions of electrolytes exist in the solvated form and the degree of solvation of the electrolytes is very sensitive to the environment temperature. It is very difficult for the electrolytes to achieve complete desolvation under low temperature. Therefore, the size of the ions of the incomplete desolvate electrolytes

under low temperature is larger than that under RT, which would cause the mismatch of the pore size and the electrolyte size. For the same electrolyte, the mass transfer resistance at low environment temperature would be much higher than that at RT which result in the loss of capacitance. To achieve the high capacitance retention under low environment temperature, it is critical that the pore size of electrode materials matches well with solvated ions in the electrolyte when the supercapacitator is operated at low environment temperature.[1,2]

**Supporting Table**

**Table S1** Physical parameters of ACN and DIOX solvents.[3,4]

| **Solvent composition** | **Dielectric constant** | **Donor number* (kcal/mol)** | **Melting point (°C )** | **Viscosity at 25°C (cP)** |
|---|---|---|---|---|
| ACN | 37.5 | 14.1 | -45 | 0.34 |
| DIOX | 6.8 | 18.0 | -95 | 0.58 |

**References**


1. J. Xu, N. Y. Yuan, J. M. Razal, Y. P. Zheng, X. S. Zhou, J. N. Ding, K. Cho, S. H. Ge, R. J. Zhang, Y. Gogotsi, R. H. Baughman, *Energy Storage Mater*. **2019**, *2*, 323-329.
2. J. Chmiola, G. Yushin, Y. Gogotsi, C. Portet, P. Simon, P. Taberna, *Science*, **2006**, *313*, 1760-1763.
3. I. M. Smallwood, Handbook of organic solvent properties. *Butterworth-Heinemann* **2012**.
4. C. Pean, B. Daffos, B. Rotenberg, P. Levitz, M. Haefele, P. L. Taberna, P. Simon, M. Salanne, *J. Am. Chem. Soc.* **2015**, *137*, 12627-12632.